Lewis Pairs as Highly Tunable Dynamic Crosslinks in Transient Polymer Networks

Fernando Vidal, John Gomezcoello, Roger A. Lalancette, and Frieder Jäkle*

Department of Chemistry, Rutgers University-Newark, 73 Warren Street, Newark, New Jersey 07102, United States.

KEYWORDS: Lewis Pairs, Organoboranes, Polymers, Supramolecular Chemistry, Transient Polymer Networks.

ABSTRACT: Classical Lewis pairs (LPs) between unhindered electron-poor Lewis acids (LAs) and electron-rich Lewis bases (LBs) present an overlooked motif with tremendous potential as dynamic crosslinks in transient polymer networks (TPNs) for self-healing and stimuli-responsive applications. We demonstrate that simple and intuitive matching of weak/strong organoborane LA and amine LB pairs offers access to a large set of binding equilibrium constants, K_{eq}, that span ~6 orders and dissociation rate constants, k_{diss}, that span ~7 orders of magnitude. The implementation in polystyrene (PS) / polydimethylsiloxane (PDMS) blends results in dynamically crosslinked networks with bulk thermomechanical properties that are directly correlated with the strength and kinetic parameters for the LP interactions. The LP dynamic crosslink design is highly versatile and broadly applicable to different polymer architectures as demonstrated in the formation of reprocessible elastomers from Lewis base-decorated high molecular weight PDMS in combination with Lewis acid-decorated PS, when reinforced with fumed silica as a filler.

Introduction

The success of supramolecular chemistry in revolutionizing biomedicine, soft materials, molecular machines, sensors, and catalysis—to name just a few areas impacted by its implementation—relies on non-covalent interactions that give rise to self-assembly and stimuli-responsiveness as the most prominent features.[1-4] Hydrogen bonding, metal-ligand, hydrophobic/hydrophilic, host-guest, π-π stacking, and ion-ion or π-ion interactions have become essential tools to access the desired properties and functions by providing a wide variety of binding affinities and responses to external cues (Figure 1a).[5] New strategies for supramolecular polymers and networks remain in great demand as they give access to unexplored applications by expanding the range and scope of multi-stimuli-responsive materials and improving the reversibility of the interactions.[6-11]

"Classical" Lewis pairs (LPs), in which a reversible non-covalent bond is stablished between a Lewis base (e.g., N-containing electron-donor, LB) and a Lewis acid (e.g., electron-deficient organoborane, LA), are highly attractive supramolecular synthons because: (1) the binding equilibrium constant (K_{eq}) can be easily tuned by both electronic and steric modification of substituents, (2) the dative bond is highly directional and confined, and (3) the physicochemical properties can be modulated to respond to external stimuli triggered by a reversible ON/OFF switch (for instance, the absorption/emission between the bound/free states in a chromophoric LA).[12, 13] Recent advances in introducing Lewis acidic triarylboranes into the main-chain and as pendent groups of linear polymers and into covalent networks have enabled applications as polymer-bound catalysts, chemical sensors, and photoswitchable materials.[14-17] In addition, the combination of sterically hindered LAs with bulky LBs, so-called "frustrated" Lewis pairs (FLPs), has been exploited for constructing dynamic polymer networks in the presence of small molecule gelators.[18-21] However, applications of LPs in supramolecular polymeric materials remain scarce,[22-26] and scientists have yet to capitalize on the exceptional tunability and potentially vast range of binding strengths accessible with LPs (Figure 1a).

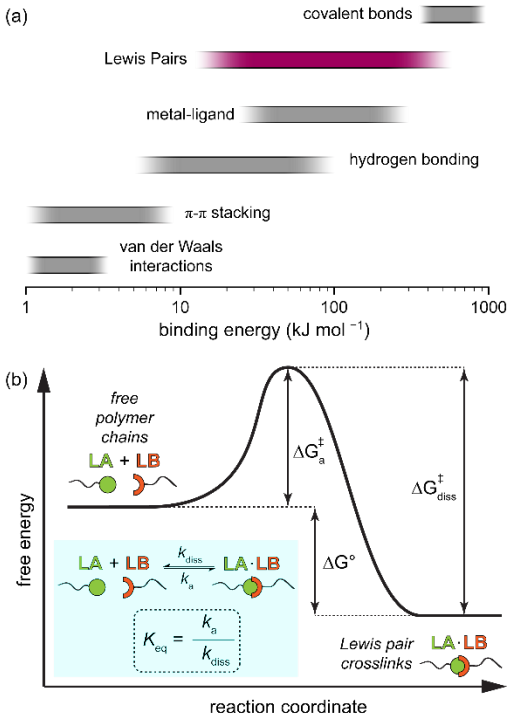

Figure 1. (a) Approximate ranges of binding energies for various types of molecular interactions (adapted from references [27, 28]). (b) Schematic energy diagram and binding equilibrium for the associative interaction between LA and LB tethered to polymer chains to form a LP crosslink.

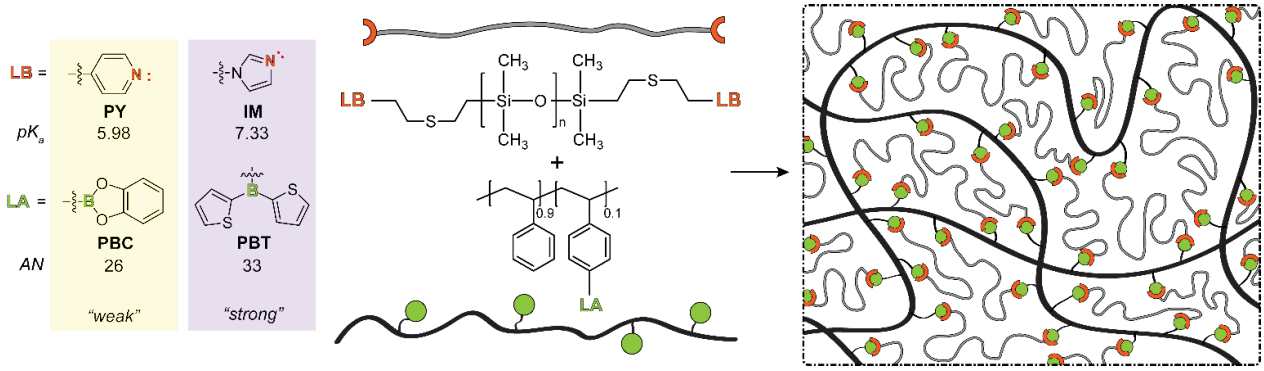

Scheme 1. Schematic representation of transient polymer networks formed between LA-containing PS (black lines) and LB-terminated telechelic PDMS (grey lines). AN = acceptor number (see SI).

Transient polymer networks (TPNs) have become an enticing platform for exploiting supramolecular interactions since the unique molecular dynamics that govern the reversibility of the network nodes, i.e. the rate of crosslink dissociation (k_{diss}), dictates the materials bulk physical properties (Figure 1b).[29-31] If the non-covalent bonds holding together the supramolecular network are sufficiently weak and readily reversible at room temperature, the materials can self-heal without further stimulus due to the rapid reorganization of the crosslinks. However, these materials usually exhibit what might be considered undesired creep. Conversely, much stronger dynamic covalent chemistries, such as Diels-Alder or transamination reactions, typically require high temperatures to undergo the stress-relaxation necessary for mending and reprocessing, a concept widely explored in vitrimers.[32-37] In this context, the tunable rates of transesterification between covalently linked boronic esters in TPNs excitingly illustrates the efficacy of small molecule organoboranes for designing new dynamic materials.[38-42] Thus, strategies that directly control the temperatures at which dynamically crosslinked materials become malleable remain highly desirable for expanding the range of applications.[43]

In this work, we set out to exploit the large variations in binding strength that can be achieved with LPs to tune the properties of TPNs (Scheme 1). To that end, we employ organoborane LAs and amine LBs that form adducts with K_{eq} and k_{diss} values that span over 7 orders of magnitude. We then show for the first time that this exceptional variability of LP strength translates into drastically different thermomechanical bulk properties of otherwise structurally similar TPNs. In addition, we demonstrate how this concept can be directly applied to generate novel silicone rubbers as industrially relevant materials.

Results and Discussion

Thermodynamic and Kinetic Parameters of Molecular Lewis Acid-Base Model Complexes. An accurate description of the kinetic and thermodynamic parameters for the formation of the dative bond between the LB and LA groups is crucial to gain a detailed understanding of the chemical equilibrium and association/dissociation dynamics of the LP crosslinks. By using isolable small molecules these non-covalent interactions can be more accurately quantified, and the adoption of such binding motifs into a supramolecular polymer network will then allow correlations with the macroscopic properties. The familiar and intuitive description of "strong" and "weak" LPs typically relies on monitoring spectroscopic changes observed upon adduct formation with reference Lewis bases.[44, 45] Accordingly, a strong LP has a large thermodynamic driving force (Gibbs free energy), which can also be verified using computational methods.[46-48] While extensive data are available for the complexation of anions to organoborane LAs,[49] quantitative binding data for neutral complexes are sparse. As Lewis acidic tricoordinate boranes to partake in the LP binding motifs, we selected [4-(*tert*-butyl)phenyl]catecholboronate (**BCat**) and (4-(*tert*-butyl)phenyl)di(thiophen-2-yl)borane (**BTh_2**). In the former, the presence of catechol decreases the Lewis acidity by partially populating the empty p-orbital of the boronate ester via π donation.[46, 50] The Lewis acidity of the latter is expected to be significantly higher, as qualitatively shown by the larger acceptor numbers, AN (see SI).[51-53] As model LBs we selected 4-ethylpyridine (**^{Et}Py**) and *N*-ethyl-imidazole (**^{Et}Im**) which, not accounting for steric factors, may be considered relatively "weaker" and "stronger" N-donors based on their reported Brønsted basicity (pK_a = 5.98 for 4-picoline and 7.33 for 1-methyl imidazole).[54, 55]

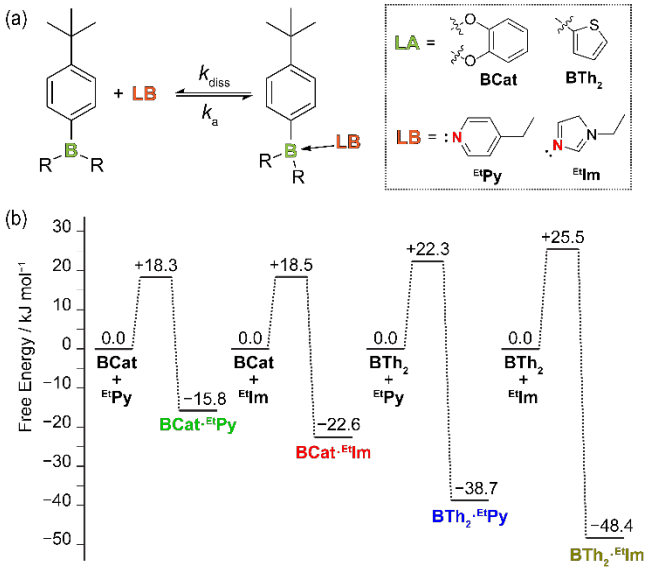

Figure 2. (a) LP binding equilibrium between model tricoordinated organoboranes (LAs) and N-heterocyclic LBs. (b) Schematic free energy diagram (as described in Figure 1b) derived from the experimentally determined equilibrium constants ($\Delta G°$, Table S4) and activation energies ($\Delta G^{\ddagger}_{diss}$, Table S5) of the model LP adduct formation, $\Delta G^{\ddagger}_{a} = \Delta G° - |\Delta G^{\ddagger}_{diss}|$.

When mixing equimolar amounts of these model LBs and LAs at room temperature LP equilibria were established instantaneously, indicative of a low kinetic barrier for the associative process (Figure 2a). The ^{11}B NMR chemical shifts of the mixtures (0.1 M in $CDCl_3$) experienced an upfield shift (new resonances between 15.8 and −3.8 ppm) accompanied by a significant line narrowing, both clear indications of (at least partial) formation of tetracoordinated borate complexes (Table S3 and Figures S77–S88). Notably, the magnitude of the shifts followed the anticipated relative strength of the components. Thus, the ^{11}B NMR resonance of the boronate in **BCat** experienced smaller shifts compared with the more Lewis acidic arylborane in **BTh$_2$**; complexes with the weaker **^{Et}Py** provoked smaller shifts than the stronger **^{Et}Im** (Table S3). The poor solubility of the Lewis pairs in non-polar hydrocarbons, such as hexanes and pentane, allowed their isolation and complete spectroscopic characterization (see SI). Single crystal X-ray analyses confirmed the expected distorted tetrahedral geometry of the tetracoordinated catecholborates and the B-N distances were in the typical range of dative bonds (Table S3 and Figures S1-S2). To quantify the adduct formation, binding constants were determined by UV-titration experiments for each of the LPs (Table 1, see SI for experimental details). The K_{eq} differed by over 6 orders of magnitude from 6×10^2 M^{-1} to 3×10^8 M^{-1} (**BCat·^{Et}Py** < **BCat·^{Et}Im** < **BTh$_2$·^{Et}Py** < **BTh$_2$·^{Et}Im**). These results highlight the impact of the combined LA and LB strength in the binding equilibrium, generating a wide range of binding energies ($\Delta\Delta G° = 32.6$ kJ mol^{-1}, Figure 2b and Table S4) that covers much of that for typical non-covalent bonds achieved by hydrogen bonding, metal-ligand, or host-guest interactions in one single system.[5, 31] Within the specific models tested in this study, it is mainly the nature of the LA rather than the LB that determines the overall magnitude of the binding affinity, while the LB serves as a modulator to further tune the level of K_{eq}. We anticipate that higher Lewis acidities, for instance by introducing electron-withdrawing fluoroaryl substituents, could lead to even larger values of K_{eq}.[46, 56]

Not only the equilibrium constants, but also the kinetics of crosslink formation and cleavage are expected to have a dramatic impact on the network dynamics. To verify the dynamic nature of the LP adduct formation and to deduce the respective kinetic parameters we performed variable temperature ^{1}H NMR experiments on mixtures containing the LPs with one additional equivalent of LB ([LB]/[LA] = 2:1, see SI). The collected spectra clearly demonstrate that an exchange equilibrium between free and bound N-donor is established and permit the quantitative determination of k_{diss} values by lineshape analysis (values at 25 °C are summarized in Table 1 and Table S5). The data thus obtained confirms the expected reciprocity between K_{eq} and k_{diss}, i.e., the lowest binding affinities provide for the fastest exchange dynamics and vice versa. Remarkably, the exchange rate of the weakest LP with additional LB (**BCat·^{Et}Py** and **^{Et}Py***, $k_{diss} = 6.5 \times 10^6$ s^{-1}) is almost 7 orders of magnitude faster than that of the strongest LP (**BTh$_2$·^{Et}Im** and **^{Et}Im***, $k_{diss} = 6.9 \times 10^{-1}$ s^{-1}). The calculated associative rate constants, $k_a = K_{eq} \times k_{diss}$, indicate that the formation of the unhindered LPs is in fact diffusion controlled in all cases ($k_a > 10^8$ s^{-1}), and this explains the inverse correlation between K_{eq} and k_{diss}. A glance at the thermodynamic landscape constructed with the experimental binding free energies, ΔG°, and activation free energies of the dissociation process, $\Delta G^{\ddagger}_{diss}$, further illustrates how the low activation barrier of the forward reaction (18.3–25.5 kJ mol^{-1}) permits the instantaneous establishment of the binding equilibrium at room temperature (Figure 2b). Thus, with little to no steric hindrance and complementary tunability of both the borane Lewis acidity and N-donor basicity, the LP design offers direct control of the exchange dynamics over a remarkable range of dissociation rates by simple and intuitive chemical tuning of the LA-LB affinity.

Table 1. Dynamic parameters of model Lewis pairs and selected rheological properties of corresponding polymer networks prepared at [LA]/[LB] = 1.

Gel	LB	LA	K_{eq} [a] (M^{-1})	k_{diss} [b] (s^{-1})	PS wt%	η_0 [c] (Pa·s)	τ [d] (s)	T_{cross} [e] (°C)
Py-PBC	Py	BCat	6×10^2	6.5×10^6	11.1	8.4×10^2	0.14	−4.2
Im-PBC	Im	BCat	8×10^3	3.4×10^5	11.1	4.6×10^4	4.6	29.6
Py-PBT	Py	BTh_2	6×10^6	1.3×10^2	11.6	1.1×10^6	79	41.2
Im-PBT	Im	BTh_2	3×10^8	6.9×10^{-1}	11.6	1.9×10^7	>628	66.0

[a]Determined by UV-vis titration experiments in CH_2Cl_2 at 25 °C; data for **Py-PBT** and **Im-PBT** were obtained by competitive displacement of a weaker Lewis acid (see SI). [b]Determined by lineshape analysis of ^{1}H NMR traces at varied temperatures. [c]Taken from the low frequency plateau of time-temperature-superposition (TTS) mastercurves (referenced to 25 °C) in oscillatory shear measurements. [d]$\tau = 2\pi/\omega$, in oscillatory frequency sweeps (25 °C, 1% strain). [e]Obtained from a temperature ramp of 1 °C/min (1% strain, 1.0 rad/s).

Preparation of LP Polymer Formulations. The implementation of the LPs as transient crosslinks in polymer networks requires two complementary polymers carrying, respectively, the LB and LA recognizing units (Scheme 1). As flexible network bridges, we selected telechelic polydimethylsiloxane (PDMS) below its critical molecular weight (M_n < 10 kDa)[57, 58] to connect two LB units situated at the chain terminus, pyridine (**Py**) or imidazole (**Im**). As the network nodes, we chose linear polystyrene functionalized with pendant catecholboronates (**PBC**) or di(thiophen-2-yl)boranes (**PBT**) randomly distributed along the backbone (on average ca. 17 LA units per chain), capable of acting as multi-crosslinking strands. The advantages of using PDMS/PS polymer blends are multiple-fold: (1) the low melting transition of the PDMS chains ensures the viscous flow necessary for the rheological response of the network while allowing the diffusion of the recognizing units without the use of organic solvents, (2) the high glass transition temperature of the PS chains provides added stiffness to the resulting viscoelastic materials and offers an opportunity for the fabrication of mechanically robust elastomers, (3) the inherent immiscibility of the two polymers exerts an entropically driven microstructure that seeks to minimize the PS/PDMS interface. The use of post-functionalization methods to prepare the PS and PDMS polymers from common parent precursor polymers ensured that the number average molecular weight (M_n), polymer dispersity ($Đ$), and the average number of functional groups per chain (F), is comparable across the chosen LA and LB polymers, maximizing reliability of comparative studies on the rheological and thermomechanical properties. Table S1 summarizes the characteristics of the polymers employed in this study and a full description of polymer synthesis and characterization is provided in the SI.

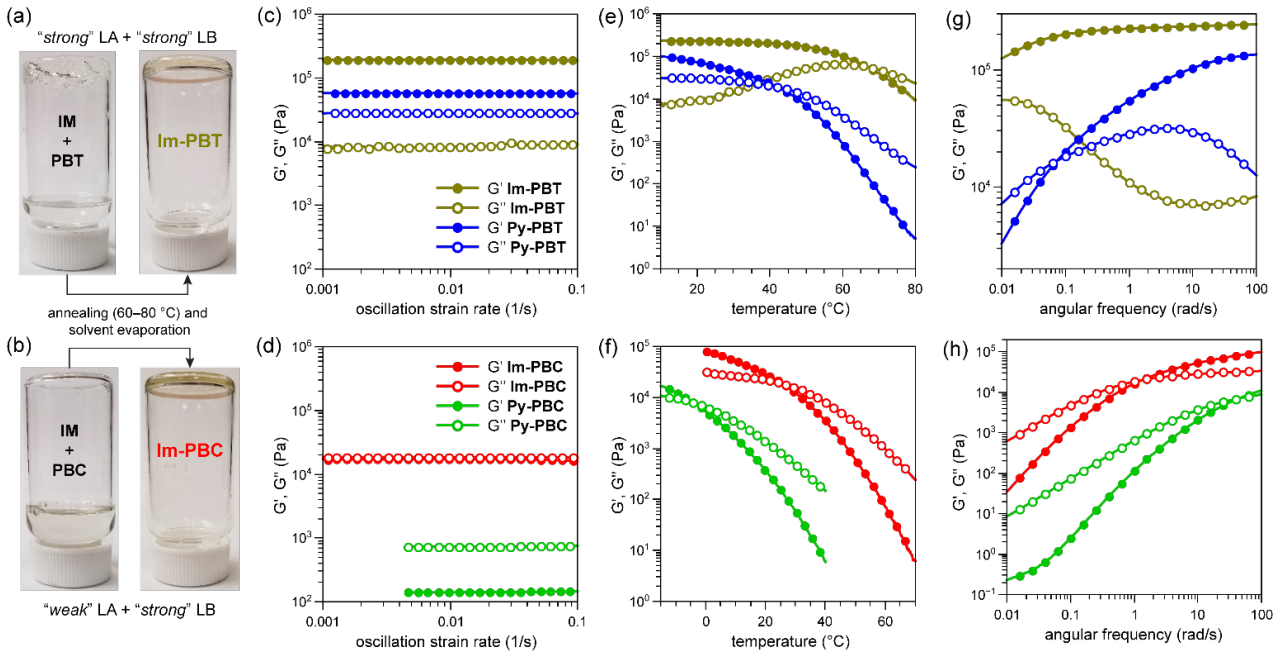

Figure 3. Representative photographs taken during the preparation of formulations: (a) **Im-PBT** (notice the toluene/CH_2Cl_2 mixture phase-separated from the organogel) and (b) **Im-PBC** (homogeneous free flowing solution) before and after solvent evaporation; viscoelastic moduli G' (filled circles) and G'' (empty circles) for PS/PDMS networks **Im-PBT** (olive), **Py-PBT** (blue), **Im-PBC** (red), and **Py-PBC** (green) measured by (c, d) dynamic stress sweep (25 °C, 1.0 rad/s), (e, f) temperature sweep (1 °C/min, 1% strain, 1.0 rad/s, and (g, h) frequency sweep (25 °C, 1% strain) experiments.

The differences in the dynamics of supramolecular crosslinking, modeled by the interactions described above, became immediately apparent when polymer solutions (CH_2Cl_2/toluene solvent mixture) containing the recognition units in a 1:1 molar ratio of [LA] to [LB] were mixed at room temperature. At the polymer concentrations employed (~ 4–5 g dl^{-1}), formulations **Py-PBT** and **Im-PBT**, containing the more highly Lewis acidic **BTh_2** binding sites, instantaneously gelled. Contrarily, formulations **Py-PBC** and **Im-PBC**, containing the weaker **BCat** sites, remained free flowing (Figures 3a,b). These employed semi-dilute conditions accentuated the differences between the binding equilibria established at room temperature. The lower binding affinities and faster exchange rates associated with **BCat** created fewer crosslinking points and the rapid dissociation of the network nodes resulted in relatively low viscosities. On the other hand, the much higher K_{eq} and lower k_{diss} of **PBT** complexes effectively locked the polymer chains to create a disordered three-dimensional network. Upon relaxation, accelerated by high temperature annealing at 60–80 °C, mixtures of **PBT** and **Py**/**Im** became highly viscous. Finally, after solvent evaporation, all polymer blends, containing 11.1–11.6 wt% PS, appeared as homogeneous, transparent, and lightly yellow colored gels of varying stiffness.

The homogeneity and transparency of the formulations points to the advantageous role of the LPs as supramolecular compatibilizers, allowing the solubilization of PS chains into the PDMS domains and thus forming a single homogeneous melt phase (Scheme 1). Other blends of PS/PDMS with supramolecular bonds have been reported to spontaneously self-assemble into complex architectures due to the high immiscibility of the two polymer types when carefully selecting the topological connectivity.[59-61] In our case, wide-angle X-ray scattering (WAXS) and small-angle X-ray scattering (SAXS) diffractograms of **Py-PBT** and **Im-PBT** networks displayed similar broad and isotropic patterns, indicative of amorphous and homogeneous phases that are not dependent on the nature of the LP (Figures S65-S66 and Table S6).[62, 63] In addition, differential scanning calorimetry (DSC) thermograms of the dry networks (Figures S55-S58) during the first heating scan (−90 °C to 200 °C) revealed a characteristic melting transition, T_m, at −50 °C due to the PDMS domains but no distinct glass transition, T_g, that could be attributed to a separate PS domain (T_g of borylated PS occur at 117–118 °C).

If the stability of the PS/PDMS single-phase is concomitant to the strength of the Lewis adduct, then sufficient weakening of the LP interaction should render the two phases incompatible as the unfavorable free energy of mixing overcomes that of the supramolecular network. Indeed, elevated temperatures promoted macroscopic phase-segregation in dry networks containing the weaker LPs (150 °C and 200 °C for **Py-PBC** and **Im-PBC**, respectively, Figures S60-S61). In contrast, formulations containing a stronger LA remained transparent (**Im-PBT**) or almost completely homogeneous (**Py-PBT**) at temperatures closer to 200 °C due to higher concentration of effective crosslinks provided by the stronger LPs (Figures S62-S63). Such irreversible and thermally induced phase-separation explains the appearance of a weak T_g (~120 °C) in the second heating scan of the DSC thermograms of formulations containing **BCat** binding sites, but not those containing the stronger **BTh_2**. A control experiment with a competing molecular LB illustrated a similar network weakening effect. Adding a few drops of **^{Et}Im** to a solution containing **Py-PBT** generated a phase segregated mixture of solid PS and liquid PDMS after removing the solvent. Thus, complexation of the pendant triarylboranes in the PS chains with the untethered **^{Et}Im**, whose binding affinity is ca. 50 times larger than that of pyridine, rendered the two polymers macroscopically incompatible and their mixture heterogenous.

To further verify the Lewis pair formation within the polymer network, **Py-PBT** organogels in $CDCl_3$ (15 g dl^{-1}) were prepared in 2:1 and 1:1 [LA]/[LB] ratios. Comparing the ^{11}B NMR signals with those of a mixture of polymer **PBT** with the molecular LB, ^{Et}**Py**, under otherwise identical conditions, provided further evidence of the binding between the pendant **BTh₂** units in the PS chains and the pyridine groups at the PDMS termini (Figure S91). The broad signal of **PBT** centered at 52.8 ppm almost completely disappeared with only 1 equivalent of LB added, indicating a high degree of capping of the organoborane binding sites. Considering the associative K_{eq} of the binding pairs (> 10^2 M^{-1}) and the concentration of LP sites in the final formulations (ca. 0.09 M), the expected degree of B←N bond fulfillment after solvent evaporation is high in all cases (~90% for the weakest pair, **Py-PBC**, and >96% for all others).[64] Hence, the degree of crosslinking in the formulations is expected to be comparable and high in all cases.

Rheological Studies of LP Crosslinked Polymer Networks. We first examined the viscoelastic properties of the dry gels by dynamic oscillatory rheology in the region of linear response. An excellent correlation of the reversible dynamics of LP dissociation with the observable mechanical properties was found. The zero shear viscosities, η_0, a measure of the material viscosity at rest, exponentially increased over 4 orders of magnitude from 840 Pa·s for **Py-PBC** to 19 MPa·s for **Im-PBT** (Table 1), despite the only marginal variations in PS content (~0.5 wt%). The impact of the LP binding affinity and LB exchange kinetics on η_0 is remarkable and essential to explain the observed trends, considering that almost 90 wt% of the gels consist of low viscosity unentangled PDMS chains (in comparison, the η_0 of **Py** and **Im** are 0.17 and 0.23 Pa·s, respectively). A closer look at the storage (G') and loss (G'') moduli, the elastic and viscous components of the viscoelastic modulus, offers further insight into the solid-like or fluid-like behavior of the materials (Figures 3c,d). The observation that G' > G'' for **Im-PBT** and **Py-PBT** signifies the ability of the polymer network to reversibly store the deformation energy during the oscillatory stress, similar to the purely elastic response of covalently crosslinked rubbers. The solid-like nature of the networks derived from the strongest LPs arises from structural nodes of the network with lifetimes that are greater than the time-scale of the oscillatory deformation. Conversely, the relaxation of the **Py-PBC** network, containing the weakest of the LPs tested, is clearly dominated by viscous dissipation as shown by G''>G', a characteristic of fluid-like materials. In this case, the nodes break and reform more frequently than the stress is applied. Interestingly, **Im-PBC** presents a unique case in which G'~G''—it stores as much elastic energy as it dissipates by viscous flow—since the reciprocal time scale of the network relaxation (*vide infra*) approximately coincides with the frequency of the oscillatory experiment (1.0 rad·s^{-1}).

Since the dynamics that determine the crosslink relaxations are governed by the activation energy of the LP dissociation, the response of the networks must be also temperature dependent. Indeed, G' and G'' decrease upon heating (1 °C min^{-1}, strain 1%, 1 rad s^{-1}) as the kinetic energy provided to the supramolecular bonds allows faster exchange between crosslinks and results in lower moduli (Figures 3e,f). Modulus crossovers (G' = G'') were clearly detected for all the PS/PDMS formulations, with the highest temperatures achieved for the strongest LPs in **Im-PBT** (T_{cross} = 66.0 °C), followed by **Py-PBT** (T_{cross} = 41.2 °C), **Im-PBC** (T_{cross} = 29.6 °C), and **Py-PBC** (T_{cross} = −4.6 °C). For comparison, the coalescence temperatures in the variable temperature 500 MHz ^1H NMR experiments of the competing binding equilibria decrease in the same order, approximately from 80 °C, 35 °C, −20 °C, to −55 °C for **BTh₂·^{Et}Im**, **BTh₂·^{Et}Py**, **BCat·^{Et}Im**, and **BCat·^{Et}Py** respectively, albeit spread over a larger temperature range. A low temperature plateau in the G' modulus was observed for **Im-PBT** (230 kPa), where the slow dissociation rates give rise to a network with characteristics typical of fixed covalent crosslinks. Values of G' between 10-100 kPa are measured for the other networks at low temperature without reaching a plateau under the conditions tested. Importantly, we find a good overlap of the modulus curves in consecutive heating and cooling ramps, indicating excellent recovery of the mechanical properties and air/thermal stability of the polymer networks (Figure S42).

The transition from a solid-like behavior under deformations on the short time-scales (high frequencies) to a viscous-like response on the longer ones (low frequencies) is a staple of TPNs, as these macroscopic characteristics originate from the time-dependency of the non-covalent crosslink cleavage and reformation. Indeed, oscillatory frequency sweep experiments (100–0.01 rad s^{-1}, 1.0% strain, 25 °C) confirmed the dependence of the PS/PDMS viscoelastic properties on the dissociation rate of the LP bonds (Figures 3g,h). The modulus crossover, which correlates the experimental oscillatory frequency with the relaxation time of the bulk material, τ, dramatically decreases with increasing binding affinity: **Py-PBC** (45.7 rad·s^{-1}), **Im-PBC** (1.36 rad·s^{-1}), **Py-PBT** (0.075 rad·s^{-1}), and **Im-PBT** falls below the instrument limit (< 0.01 rad·s^{-1}).[65] Time-temperature-superposition (TTS) allowed us to explore frequencies beyond those limited by the rheometer. Indeed, frequency sweeps at 5 °C intervals could be successfully shifted into single mastercurves (Figures S47-S54). The modulus plateau, G', at higher frequencies (> 10^3 rad/s) for formulations **Im-PBC**, **Py-PBT**, and **Im-PBT** was high and almost identical (1.2−1.4 ×10^5 Pa), approaching that of a covalently crosslinked network. The weakest network, **Py-PBC**, required lower temperatures than those achieved experimentally (< −10 °C) to reach a plateau and thus the highest G' was somewhat underestimated (6.5 ×10^4 Pa).

Encouraged by these results we scaled the viscoelastic parameters (G', G'' and η^*) with k_{diss}. Such a correlation is viewed as a hallmark of supramolecular dynamics, as it implies that crosslink dissociation controls bulk network relaxation.[66, 67] Gratifyingly, the corresponding mastercurve (Figures 4 and S40–S41) connects the major component of the network relaxation with the scale of LP dissociation kinetics derived from the molecular model systems. The match, even though not perfect, is striking considering the complex and competing melt relaxations by the immiscible blends of PDMS and PS chains.[68] The high but not quantitative fulfillment of the **BCat·Py** pairs in the **Py-PBC** formulation compared to the other stronger LPs may explain the slightly lower than expected scaling of the viscoelastic parameters.

A potential application of these networks as self-healing materials takes advantage of the dynamic nature of the LPs as a means to repair a macroscopic rupture: as the network breaks predominantly at the weakest supramolecular bonds, the diffusion of the unbroken soft polymer strands (*via* viscous flow) allows the reformation of identical supramolecular motifs across the wound. Step-strain experiments offer clear evidence of the gels' ability to regain the initial viscoelastic modulus after a large shear strain of 200% has been applied (Figures S43–S46). Temperature-assisted (30–90 °C) shear rheology was employed

to encourage the viscous flow of the PDMS strands and accelerate the rate of crosslink dissociation, and the results indicate excellent and rapid modulus recovery when returning to room temperature and low strain values. As a result of the slow creep, two macroscopic pieces of **Py-PBT** gels ([LA]/[LB] = 1) cut to approximate square shapes and subsequently placed on a flat surface with their edges touching spontaneously rejoined after standing for approximately 2 weeks undisturbed at room temperature (Figure 5).

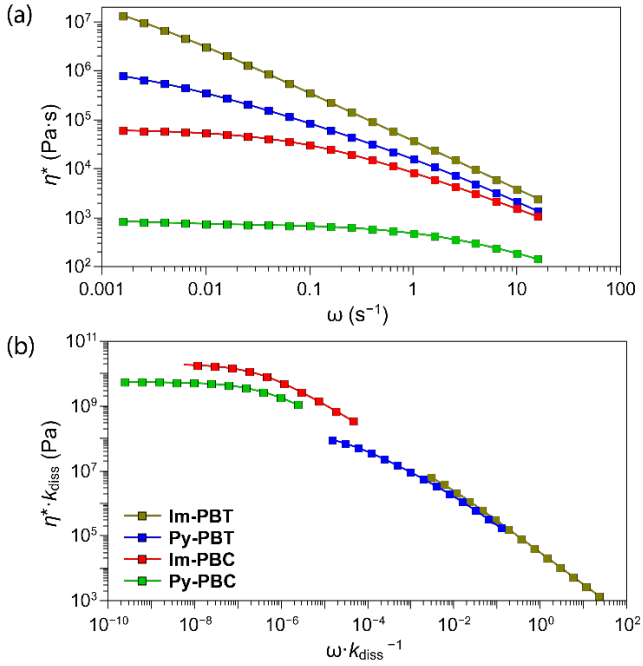

Figure 4. (a) Complex viscosity, η^*, of PS/PDMS formulations with LP crosslinks obtained by frequency sweeps (25 °C, 1.0 % strain); (b) η^* data scaled by k_{diss} measured for LP model compounds.

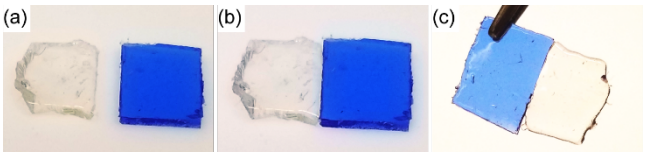

Figure 5. Self-healing visualization of **Py-PBT**: (a) separated macroscopic pieces (blue formulation stained with crystal violet during polymer mixing), (b) brought into contact at the flat edge, and (c) mending of the gap between the pieces after left in contact undisturbed for 2 weeks.

Application to Reprocessible Silicone Elastomers. Despite the appeal that TPNs offer in organo- and hydrogels to control their relaxation dynamics, the mechanical properties in the swollen state are typically weak. Such characteristics are in fact sought in biomedicine, where they have found niche applications as injectable media, slow release drug carriers, or regenerative frameworks.[69] However, the utility of new supramolecular motifs for the fabrication of mechanically robust materials, which could be employed in stimuli responsive and/or mechanosensors, requires their successful implementation into more design-specific architectures. We envisioned that by distributing pendent LBs along the backbone of a high molecular weight silicone, a more robust crosslinked rubber could be achieved in combination with the LA-functionalized PS polymers. This strategy is reminiscent of the vulcanization process: the transient LP crosslinks act on the short time scales as strong covalent bonds between elastic (entangled) strands, enabling the polymer network to sustain large elongations and stresses without break, but with the added benefit of thermal reversibility to allow for desirable recycling and reprocessing. To demonstrate this strategy, a commercially available multivinyl-containing PDMS polymer was quantitatively functionalized with pendant pyridyl groups using a "click" synthesis approach similar to that described for the telechelic polymers (M_n = 409 kDa, $Đ$ = 1.48, 0.54 mol% of pyridine, **HPy**, see SI for experimental details). Solution processing of **HPy** with **PBT** ([LA]/[LB] = 1, 8 wt%) and silica nanoparticles (Aerosil R106, 1 wt%) followed by solvent casting, yielded translucent and elastic films (Figures 6a-c). The result is a silicone rubber that is *doubly reinforced* by the combined effect of dispersing the PS and the silica filler in the polymer network, the latter being an industrial practice to reinforce rubbery materials. The homogeneity of the polymer film and uniform distribution of the nanoparticles, indicating the compatibility of both strengthening agents, is clearly visible by SEM imaging (Figure 6d). Such (nano)composite materials can sustain considerable strains (>400%) without breaking nor significant yielding, as shown by the manual stretching and elastic recovery of a film specimen (Figures 6b,c). Tensile-testing experiments showed a significant strain-hardening typical of crosslinked silicone rubbers; in sharp contrast the **HPy**+silica blend was permanently deformed (flow) with no increase of the applied force (Figure 6e). Further characterization by dynamic mechanical analysis (DMA) of the elastic films confirmed the presence of a glassy plateau (E' = 3.6 × 10^3 MPa), a T_g (−113 °C) and a T_m (−36 °C) followed by a rubbery plateau (E' = 0.6 MPa at 25 °C) as expected for a crosslinked elastomer with PDMS domains (Figure S70). At temperatures closer to 100 °C, weakening of the LP bonds decreases the measured modulus and the elasticity corresponds to that of an entangled polymer/silica composite. In comparison, a blend of uncrosslinked **HPy**+silica displays a steady decrease of E' above the T_m due to the flow of entangled PDMS chains. Stress relaxation experiments qualitatively showed the temperature dependence of the relaxation modulus, G(t): only 90 minutes after a rapid 20% strain spike, G(t) had decreased by 68% (60 °C) and 84% (90 °C) with respect to the value of G(t) at 30 °C (Figure 6f). While permanently crosslinked silicone rubbers show little stress relaxation, the flow of PDMS chains in response to the tensile deformation becomes possible due to the reversibility of the LP crosslinks. Finally, small pieces of scrap film material could be easily melt-reprocessed at 100 °C into a single film (Figure S68). The excellent recovery of the initial mechanical properties is illustrated by the regained storage modulus, E', to almost the initial values in a DMA frequency sweep experiment (Figure 6g).

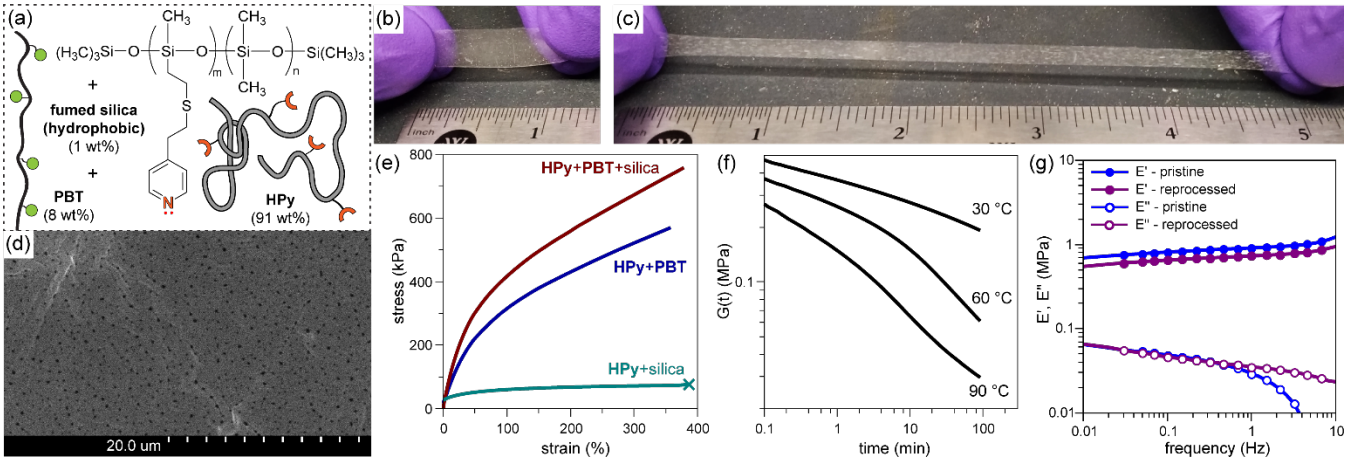

Figure 6. (a) Composition of **HPy**+**PBT**+silica reinforced silicone rubber containing LP crosslinks. (b and c) Photographs of a rectangular specimen (0.5 mm thick) of (nano)composite silicone rubber at rest and under >400% strain (reference scale in inches). (d) Scanning electron micrograph of the bulk rubber material **HPy**+**PBT**+silica showing the dispersion of the reinforcing silica nanoparticles (1 wt%). (e) Tensile-testing of **HPy**+silica(1 wt%) blend and crosslinked rubbers (elastomer specimens did not break under the testing conditions, 10 N min^{-1}). Dynamic mechanical characterization of **HPy**+**PBT**+silica(1 wt%) in tensile mode: (f) stress-relaxation (20% strain peak-hold), and (g) frequency sweeps (1% strain, 30 °C).

Conclusions

In summary, we have shown that the combination of unhindered LPs as crosslinking motifs in the construction of transient polymer networks allows for the tuning of their mechanical properties over a wide range. The small energies of activation of the associative process lead to a close correlation between the K_{eq} and k_{diss} values, which in turn dictate the dynamics of the network relaxations. The application of reversible LPs to more sophisticated materials only requires the adequate decoration of functional polymers tailored for their desired functions, as illustrated by the construction of reprocessible nano-reinforced silicone rubbers.

ASSOCIATED CONTENT

Supporting Information

The Supporting Information is available free of charge on the ACS Publications website.

Experimental details and additional figures (PDF)

Crystallographic data (cif)

AUTHOR INFORMATION

Corresponding Author

* fjaekle@newark.rutgers.edu

Author Contributions

The manuscript was written through contributions of all authors. All authors have given approval to the final version of the manuscript.

Funding Sources

NSF CHE-1609043, CRIF-0443538, MRI-1229030, 140078; Rutgers University SEED grant (202607) & Research Council; New Jersey Higher Education Equipment Leasing Fund (ELF III 047-04)

Notes

The authors declare no competing financial interests.

ACKNOWLEDGMENT

This material is based upon work supported by the National Science Foundation (NSF) under Grant CHE-1609043, a Rutgers University SEED grant (202607), and a grant from the Rutgers University Research Council. J. G. gratefully acknowledges receiving a research stipend from the NSF through the Garden State-LSAMP (NSF Award 1400780). The Bruker 500 MHz NMR spectrometer (MRI-1229030) and the X-ray diffractometer (CRIF 0443538) used in this study were acquired with support by the NSF and Rutgers University. Equipment in the Polymer and Nanomaterials Facility at Rutgers University Newark (PolyRUN) was acquired with support by the New Jersey Higher Education Equipment Leasing Fund (ELF III 047-04) and maintained with support from Rutgers University through SEED grant 202607. We thank Dr. Chunmeng Lu (New Jersey Institute of Technology) for assistance and access to hot-press instrumentation at the Polymer Processing Institute at NJIT and Dr. Nathan Rabideaux (Rutgers University-Newark) for assistance with SEM analyses of the elastomer specimens. We thank Dr. Jing Qu and Dr. Gerald Poirier at the Advanced Materials Characterization Laboratory (University of Delaware) for assistance in during DMA and SAXS/WAXS experiments. We thank Evonik Industries for a research gift of Aerosil R106 silica nanoparticles.

REFERENCES

(1) Aida, T.; Meijer, E. W.; Stupp, S. I. Functional Supramolecular Polymers. *Science* **2012,** 335, 813-817.

(2) Yang, L.; Tan, X.; Wang, Z.; Zhang, X. Supramolecular Polymers: Historical Development, Preparation, Characterization, and Functions. *Chem. Rev.* **2015,** 115, 7196-7239.

(3) Goor, O. J. G. M.; Hendrikse, S. I. S.; Dankers, P. Y. W.; Meijer, E. W. From Supramolecular Polymers to Multi-Component Biomaterials. *Chem. Soc. Rev.* **2017,** 46, 6621-6637.

(4) Kajita, T.; Noro, A.; Matsushita, Y. Design and Properties of Supramolecular Elastomers. *Polymer* **2017,** 128, 297-310.

(5) Biedermann, F.; Schneider, H.-J. Experimental Binding Energies in Supramolecular Complexes. *Chem. Rev.* **2016,** 116, 5216-5300.

(6) Yan, X.; Wang, F.; Zheng, B.; Huang, F. Stimuli-Responsive Supramolecular Polymeric Materials. *Chem. Soc. Rev.* **2012,** 41, 6042-6065.

(7) Amaral, A. J. R.; Pasparakis, G. Stimuli Responsive Self-Healing Polymers: Gels, Elastomers and Membranes. *Polym. Chem.* **2017,** 8, 6464-6484.

(8) Calvino, C.; Neumann, L.; Weder, C.; Schrettl, S. Approaches to Polymeric Mechanochromic Materials. *J. Polym. Sci., Part A: Polym. Chem.* **2017,** 55, 640-652.

(9) Herbert, K. M.; Schrettl, S.; Rowan, S. J.; Weder, C. 50th Anniversary Perspective: Solid-State Multistimuli, Multiresponsive Polymeric Materials. *Macromolecules* **2017,** 50, 8845-8870.

(10) Sagara, Y.; Karman, M.; Verde-Sesto, E.; Matsuo, K.; Kim, Y.; Tamaoki, N.; Weder, C. Rotaxanes as Mechanochromic Fluorescent Force Transducers in Polymers. *J. Am. Chem. Soc.* **2018,** 140, 1584-1587.

(11) Sagara, Y.; Karman, M.; Seki, A.; Pannipara, M.; Tamaoki, N.; Weder, C. Rotaxane-Based Mechanophores Enable Polymers with Mechanically Switchable White Photoluminescence. *ACS Central Sci.* **2019,** 5, 874-881.

(12) Hou, Q.; Liu, L.; Mellerup, S. K.; Wang, N.; Peng, T.; Chen, P.; Wang, S. Stimuli-Responsive B/N Lewis Pairs Based on the Modulation of B–N Bond Strength. *Org. Lett.* **2018,** 20, 6467-6470.

(13) Mellerup, S. K.; Wang, S. Boron-Based Stimuli Responsive Materials. *Chem. Soc. Rev.* **2019,** 48, 3537-3549.

(14) Jäkle, F. Advances in the Synthesis of Organoborane Polymers for Optical, Electronic, and Sensory Applications. *Chem. Rev.* **2010,** 110, 3985-4022.

(15) Cheng, F.; Bonder, E. M.; Jäkle, F. Electron-Deficient Triarylborane Block Copolymers: Synthesis by Controlled Free Radical Polymerization and Application in the Detection of Fluoride Ions. *J. Am. Chem. Soc.* **2013,** 135, 17286-17289.

(16) Wang, J.; Jin, B.; Wang, N.; Peng, T.; Li, X.; Luo, Y.; Wang, S. Organoboron-Based Photochromic Copolymers for Erasable Writing and Patterning. *Macromolecules* **2017,** 50, 4629-4638.

(17) Vidal, F.; Jäkle, F. Functional Polymeric Materials Based on Main-Group Elements. *Angew. Chem. Int. Ed.* **2019,** 58, 5846-5870.

(18) Wang, M.; Nudelman, F.; Matthes, R. R.; Shaver, M. P. Frustrated Lewis Pair Polymers as Responsive Self-Healing Gels. *J. Am. Chem. Soc.* **2017,** 139, 14232-14236.

(19) Chen, L.; Liu, R.; Yan, Q. Polymer Meets Frustrated Lewis Pair: Second-Generation CO2-Responsive Nanosystem for Sustainable CO2 Conversion. *Angew. Chem.* **2018,** 130, 9480-9484.

(20) Chen, L.; Liu, R.; Hao, X.; Yan, Q. CO2-Cross-Linked Frustrated Lewis Networks as Gas-Regulated Dynamic Covalent Materials. *Angew. Chem. Int. Ed.* **2019,** 58, 264-268.

(21) Yolsal, U.; Wang, M.; Royer, J. R.; Shaver, M. P. Rheological Characterization of Polymeric Frustrated Lewis Pair Networks. *Macromolecules* **2019,** 52 (9), 3417-3425 DOI: 10.1021/acs.macromol.9b00271.

(22) Sheepwash, E.; Luisier, N.; Krause, M. R.; Noé, S.; Kubik, S.; Severin, K. Supramolecular Polymers Based on Dative Boron–Nitrogen Bonds. *Chem. Commun.* **2012,** 48, 7808-7810.

(23) Dodge, L.; Chen, Y.; Brook, M. A. Silicone Boronates Reversibly Crosslink Using Lewis Acid– Lewis Base Amine Complexes. *Chem.-Eur. J.* **2014,** 20, 9349-9356.

(24) Luisier, N.; Schenk, K.; Severin, K. A Four-Component Organogel Based on Orthogonal Chemical Interactions. *Chem. Commun.* **2014,** 50, 10233-10236.

(25) Luisier, N.; Scopelliti, R.; Severin, K. Supramolecular Gels Based on Boronate Esters and Imidazolyl Donors. *Soft Matter* **2016,** 12, 588-593.

(26) Vidal, F.; Lin, H.; Morales, C.; Jäkle, F. Polysiloxane/Polystyrene Thermo-Responsive and Self-Healing Polymer Network via Lewis Acid-Lewis Base Pair Formation. *Molecules* **2018,** 23, 405.

(27) Mendes, A. C.; Baran, E. T.; Reis, R. L.; Azevedo, H. S. Self-Assembly in Nature: Using the Principles of Nature to Create Complex Nanobiomaterials. *Wiley Interdiscip. Rev.-Nanomed. Nanobiotechnol.* **2013**, *5*, 582-612

(28) Van Ruymbeke, E. Preface: Special Issue on Associating Polymers. *J. Rheol.* **2017,** 61, 1099-1102.

(29) Seiffert, S.; Sprakel, J. Physical Chemistry of Supramolecular Polymer Networks. *Chem. Soc. Rev.* **2012,** 41, 909-930.

(30) Rossow, T.; Seiffert, S., Supramolecular Polymer Networks: Preparation, Properties, and Potential. In *Supramolecular Polymer Networks and Gels*, Seiffert, S., Ed. Springer International Publishing: Cham, **2015**; 1-46.

(31) Zhang, Z.; Chen, Q.; Colby, R. H. Dynamics of Associative Polymers. *Soft Matter* **2018,** 14, 2961-2977.

(32) Chen, X.; Dam, M. A.; Ono, K.; Mal, A.; Shen, H.; Nutt, S. R.; Sheran, K.; Wudl, F. A Thermally Re-mendable Cross-Linked Polymeric Material. *Science* **2002,** 295, 1698-1702.

(33) Scott, T. F.; Schneider, A. D.; Cook, W. D.; Bowman, C. N. Photoinduced Plasticity in Cross-Linked Polymers. *Science* **2005,** 308, 1615-1617.

(34) Montarnal, D.; Capelot, M.; Tournilhac, F.; Leibler, L. Silica-Like Malleable Materials from Permanent Organic Networks. *Science* **2011,** 334, 965-968.

(35) Capelot, M.; Montarnal, D.; Tournilhac, F.; Leibler, L. Metal-Catalyzed Transesterification for Healing and Assembling of Thermosets. *J. Am. Chem. Soc.* **2012,** 134, 7664-7667.

(36) Denissen, W.; Winne, J. M.; Du Prez, F. E. Vitrimers: permanent organic networks with glass-like fluidity. *Chem. Sci.* **2016,** 7, 30-38.

(37) Zou, W.; Dong, J.; Luo, Y.; Zhao, Q.; Xie, T. Dynamic Covalent Polymer Networks: from Old Chemistry to Modern Day Innovations. *Adv. Mater.* **2017,** 29, 1606100.

(38) Bapat, A. P.; Roy, D.; Ray, J. G.; Savin, D. A.; Sumerlin, B. S. Dynamic-Covalent Macromolecular Stars with Boronic Ester Linkages. *J. Am. Chem. Soc.* **2011,** 133, 19832-19838.

(39) Cromwell, O. R.; Chung, J.; Guan, Z. Malleable and Self-Healing Covalent Polymer Networks through Tunable Dynamic Boronic Ester Bonds. *J. Am. Chem. Soc.* **2015,** 137, 6492-6495.

(40) Vancoillie, G.; Brooks, W. L. A.; Mees, M. A.; Sumerlin, B. S.; Hoogenboom, R. Synthesis of Novel Boronic Acid-Decorated Poly(2-oxazoline)s Showing Triple-Stimuli Responsive Behavior. *Polym. Chem.* **2016,** 7, 6725-6734.

(41) Accardo, J.; Kalow, J. A. Reversibly Tuning Hydrogel Stiffness through Photocontrolled Dynamic Covalent Crosslinks. *Chem. Sci.* **2018,** 9, 5987-5993.

(42) Brunet, J.; Collas, F.; Humbert, M.; Perrin, L.; Brunel, F.; Lacôte, E.; Montarnal, D.; Raynaud, J. High Glass-Transition Temperature Polymer Networks harnessing the Dynamic Ring Opening of Pinacol Boronates. *Angew. Chem. Int. Ed.* **2019,** 58, 12216-12222.

(43) Chakma, P.; Konkolewicz, D. Dynamic Covalent Bonds in Polymeric Materials. *Angew. Chem. Int. Ed.* **2019,** 58, 9682-9695.

(44) Childs, R. F.; Mulholland, D. L.; Nixon, A. The Lewis Acid Complexes of α,β-Unsaturated Carbonyl and Nitrile Compounds. A Nuclear Magnetic Resonance Study. *Can. J. Chem.* **1982,** 60, 801-808.

(45) Beckett, M. A.; Strickland, G. C.; Holland, J. R.; Sukumar Varma, K. A Convenient N.M.R. Method for the Measurement of Lewis Acidity at Boron Centres: Correlation of Reaction Rates of Lewis Acid Initiated Epoxide Polymerizations with Lewis Acidity. *Polymer* **1996,** 37, 4629-4631.

(46) Sivaev, I. B.; Bregadze, V. I. Lewis Acidity of Boron Compounds. *Coord. Chem. Rev.* **2014,** 270-271, 75-88.

(47) Jupp, A. R.; Johnstone, T. C.; Stephan, D. W. The Global Electrophilicity Index as a Metric for Lewis Acidity. *Dalton Trans.* **2018,** 47, 7029-7035.

(48) Jupp, A. R.; Johnstone, T. C.; Stephan, D. W. Improving the Global Electrophilicity Index (GEI) as a Measure of Lewis Acidity. *Inorg. Chem.* **2018,** 57, 14764-14771.

(49) Wade, C. R.; Broomsgrove, A. E. J.; Aldridge, S.; Gabbaï, F. o. P. Fluoride Ion Complexation and Sensing Using Organoboron Compounds. *Chem. Rev.* **2010,** 110, 3958-3984.

(50) Adamczyk-Woźniak, A.; Jakubczyk, M.; Sporzyński, A.; Żukowska, G. Quantitative Determination of the Lewis Acidity of Phenylboronic Catechol Esters — Promising Anion Receptors for Polymer Electrolytes. *Inorg. Chem. Commun.* **2011,** 14, 1753-1755.

(51) Qin, Y.; Pagba, C.; Piotrowiak, P.; Jäkle, F. Luminescent Organoboron Quinolate Polymers. *J. Am. Chem. Soc.* **2004,** 126, 7015-7018.

(52) Jäkle, F. Lewis Acidic Organoboron Polymers. *Coord. Chem. Rev.* **2006,** 250, 1107-1121.

(53) Qin, Y.; Jäkle, F. Formation of Polymeric Lewis Acid–Lewis Base Complexes with Well-defined Organoboron Polymers. *J J. Inorg. Organomet. Polym. Mater.* **2007,** 17, 149-157.

(54) Ramsey, B. G. Substituent Effects on Imidazole Basicity and Photoelectron Spectroscopy Determined Ionization Energies. *J. Org. Chem.* **1979,** 44, 2093-2097.

(55) Shimizu, S.; Watanabe, N.; Kataoka, T.; Shoji, T.; Abe, N.; Morishita, S.; Ichimura, H. Pyridine and Pyridine Derivatives. in *Ullmann's Encyclopedia of Industrial Chemistry*, Wiley-VCH Verlag GmbH & Co. KGaA, Weinheim, Germany, **2000**, DOI: 10.1002/14356007.a22_399.

(56) Greb, L. Lewis Superacids: Classifications, Candidates, and Applications. *Chem.-Eur. J.* **2018,** 24, 17881-17896.

(57) Porter, R. S.; Johnson, J. F. The Entanglement Concept in Polymer Systems. *Chem. Rev.* **1966,** 66, 1-27.

(58) Ferry, J., *Viscoelastic properties of polymers*. 3rd ed.; Wiley: New York, 1980.

(59) Feng, E. H.; Lee, W. B.; Fredrickson, G. H. Supramolecular Diblock Copolymers: A Field-Theoretic Model and Mean-Field Solution. *Macromolecules* **2007,** 40, 693-702.

(60) Stuparu, M. C.; Khan, A.; Hawker, C. J. Phase Separation of Supramolecular and Dynamic Block Copolymers. *Polym. Chem.* **2012,** 3, 3033-3044.

(61) Prusty, D.; Pryamitsyn, V.; Olvera de la Cruz, M. Thermodynamics of Associative Polymer Blends. *Macromolecules* **2018,** 51, 5918-5932.

(62) Di Lorenzo, F.; Seiffert, S. Nanostructural Heterogeneity in Polymer Networks and Gels. *Polym. Chem.* **2015,** 6, 5515-5528.

(63) Gu, Y.; Zhao, J.; Johnson, J. A. A Unifying Review of Polymer Networks: from Rubbers and Gels to Porous Frameworks. *Angew. Chem. Int. Ed.* **2019**, DOI: 10.1002/anie.201902900.

(64) We estimate the concentration of [LA·LB] at equilibrium given the initial concentration of [LA] and [LB] in the formulations and the experimentally determined binding constants for the model systems. For instance, for 300 mg of **Py** and 37.5 mg of **PBC** (10 mol% in **BCat** sites), the approximate concentration of [LA] sites is 0.092 M given an overall polymer density of 0.97 g mL^{-1}. Then, the concentration of [**Py**·**BCat**] adducts at equilibrium is 0.080 M (K_{eq} ~ 600 M^{-1}), which represents ~90% of the initial binding sites. .

(65) A discrepancy between the magnitudes of bulk material relaxation and dilute molecular dynamics is apparent (τ spans almost 4 decades, but k_{diss} spans 7 decades). This has been observed also for other polymer networks, see reference (38) and: (a) Shen, W.; Kornfield, J. A.; Tirrell, D. A. Dynamic Properties of Artificial Protein Hydrogels Assembled Through Aggregation of Leucine Zipper Peptide Domains. *Macromolecules* **2007**, 40, 689-692; (b) McKinnon, D. D.; Domaille, D. W.; Cha, J. N.; Anseth, K. S. Bis-Aliphatic Hydrazone-Linked Hydrogels form Most Rapidly at Physiological pH: Identifying the Origin of Hydrogel Properties with Small Molecule Kinetic Studies. *Chem. Mater.* **2014**, 26, 2382-2387; (c) Tang, S.; Olsen, B. D. Relaxation Processes in Supramolecular Metallogels Based on Histidine–Nickel Coordination Bonds. *Macromolecules* **2016**, 49, 9163-9175.

(66) Loveless, D. M.; Jeon, S. L.; Craig, S. L. Rational Control of Viscoelastic Properties in Multicomponent Associative Polymer Networks. *Macromolecules* **2005,** 38, 10171-10177.

(67) Yount, W. C.; Loveless, D. M.; Craig, S. L. Small-Molecule Dynamics and Mechanisms Underlying the Macroscopic Mechanical Properties of Coordinatively Cross-Linked Polymer Networks. *J. Am. Chem. Soc.* **2005,** 127, 14488-14496.

(68) The relaxation dynamics of PDMS and PS can be generally described as Rouse-type (beads on a spring of unentangled chains) and "sticky" reptation (along a virtual tube restricted by the topological surround-ings), respectively. See references (a) Rouse, P. E. A Theory of the Linear Viscoelastic Properties of Dilute Solutions of Coiling Polymers. *J. Chem. Phys.* **1953**, *21*, 1272-1280; (b) Leibler, L.; Rubinstein, M.; Colby, R. H. Dynamics of Reversible Networks. *Macromolecules* **1991**, *24*, 4701-4707; (c) Rubinstein, M.; Semenov, A. N. Dynamics of Entangled Solutions of Associating Polymers. *Macromolecules* **2001**, *34*, 1058-1068; (d) Rubinstein, M.; Panyukov, S. Elasticity of Polymer Networks. *Macromolecules* **2002**, *35*, 6670-6686.

(69) Mann, J. L.; Yu, A. C.; Agmon, G.; Appel, E. A. Supramolecular Polymeric Biomaterials. *Biomaterials Science* **2018,** 6, 10-37.

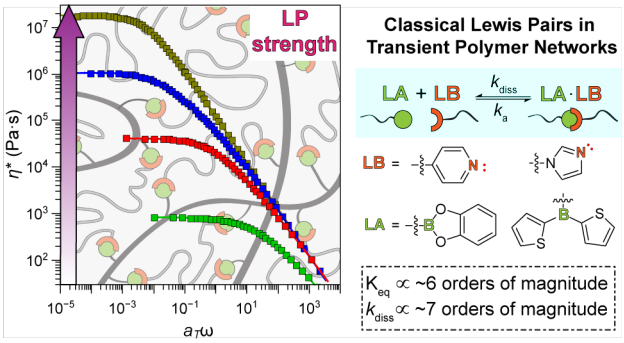
LP
strength
η^* (Pa·s)
$a_T\omega$
Classical Lewis Pairs in
Transient Polymer Networks
LA + LB
k_{diss}
k_a
LA·LB
LB =
LA =
K_{eq} ∝ ~6 orders of magnitude
k_{diss} ∝ ~7 orders of magnitude